Journal of Engineering Physics and Thermophysics, Vol. 82, No. 6, 2009

DIAGNOSTICS OF AVERAGE TEMPERATURE FIELDS AND ELECTRON DENSITIES IN A BARRIER DISCHARGE PLASMA IN THE PRESENCE OF AIR FLOW

P. P. Khramtsov, O. G. Penyazkov, V. M. Grishchenko, M. V. Doroshko, M. Yu. Chernik, and I. A. Shikh

UDC 532.517.4

We have made measurements with the optical method of the temperature and electron density distributions in an ionized gas flow induced by a high-frequency barrier discharge in the presence of air flow. Interaction with the incident flow leads to a maximum of the average-temperature distribution in the vicinity of the needle electrodes, and a maximum of the average electron density in the region of the opposite electrode.

Keywords: *aerodynamic drag, barrier discharge, plasma, shadow method.*

Introduction. The investigation of the possibilities of using plasma actuators based on dielectric barrier discharge for controlling the flow and influencing the aerodynamic drag of flying vehicles is a topical and promising direction of scientific investigations. Suffice it to say that the influence of plasma actuators on the lift coefficient proved to be comparable to the influence of flaps, but the former have the advantage of having no moving parts.

The main problems facing researchers in this field are increasing the operational efficiency of actuators and developing a physical mechanism of influence of the dielectric discharge on the aerodynamic characteristics of flows. J. R. Roth et al. [1] carried out an analysis of the properties of dielectrics most commonly used in manufacturing actuators with the aim of choosing the most optimal material characterized by minimum losses in its heating, which are sometimes comparable to the energy input into dielectric barrier discharge plasma. It was shown that the least loss was obtained in using caprolone and quartz, in which case an important role is played by the thickness of the material.

For a long time it has been thought that the decrease in the aerodynamic drag of bodies on whose surface a dielectric barrier discharge is formed is caused by the increase in the air temperature in the boundary layer; however, experimental data point to an insignificant heating in the discharge region [2, 3]. Photography of the plasma luminescence of the dielectric barrier discharge with nanosecond exposure revealed the structure of the streamers formed in it [2]. The authors of [4, 5] investigated the structure of the boundary layer formed by ionic wind and ascertained the presence of a recirculation zone in the interelectrode region.

Experimental studies of the discharge characteristics revealed a strong dependence of the induced ionic wind velocity on the form of voltage pulses applied to electrodes and their repetition rate, as well as the phenomenon of saturation of the increase in velocity with increasing voltage applied [6, 7].

The application of plasma actuators permits solving the problem of flow separation from the wing surface [8]. At angles of attack up to 5^{o} it turned out to be possible to prevent the flow separation at velocities reaching 2.85 m/sec, and as the angle of attack was increased to 15^{o}–21^{o}, the limit velocity values increased to 75 m/sec [1]. These results can find practical application in the take off and landing of flying vehicles.

In the scientific literature, there exist two approaches to the computational modeling of the dielectric barrier discharge. The first approach relies on the calculation of the mass forces arising in the discharge with account for the chemical reactions between the gas molecules and the momentum and heat transfer. The second approach is based on the representation of the plasma actuator in the form of a set of air capacitors and the calculation of mass forces on the basis of the theory on the plasma structure and the known formulas for the flat capacitor. In investigating the influence of discharge parameters and design features of the actuator on the characteristics of the ionic wind obtained, it has been established that the simulation results are in good agreement with experimental data and the plasma luminescence intensity varies depending on the voltage applied to the electrodes as $\sim V^{7/2}$ [9].

A. V. Luikov Heat and Mass Transfer Institute, National Academy of Sciences of Belarus, 15 P. Brovka Str., Minsk, 220072, Belarus. Translated from Inzhenerno-Fizicheskii Zhurnal, Vol. 82, No. 6, pp. 1125–1131, November–December, 2009. Original article submitted October 30, 2008.

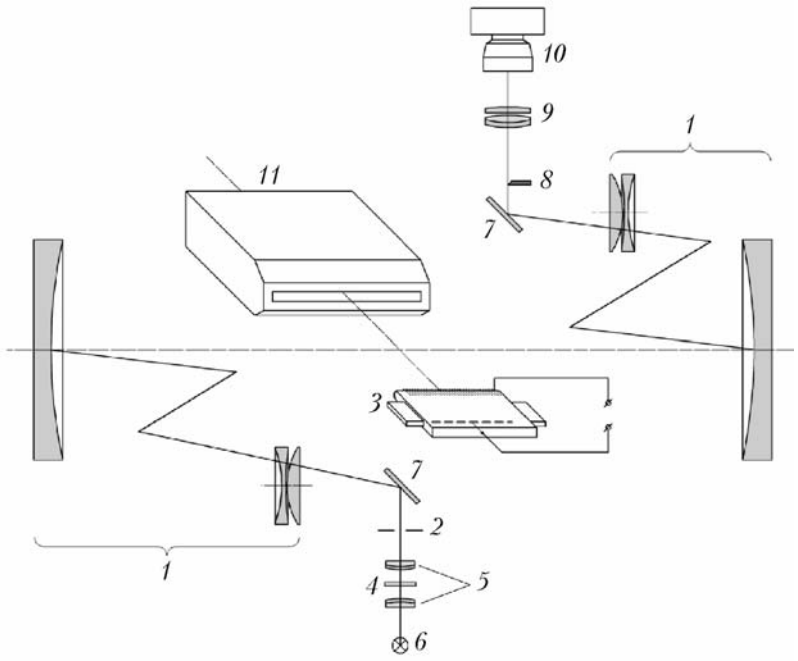

Fig. 1. Optical scheme of the experimental setup: 1) catadioptric lens; 2) slit; 3) plate; 4) optical filter; 5) capacitor; 6) DRSh 100-2 tube; 7) deflecting mirror; 8) Faucault knife; 9) lens; 10) camera; 11) nozzle.

The plasma electron density of the dielectric barrier discharge in stationary air was investigated by an optical method in [10, 11]. The method relies on the change in the optical density of the gas depending on the electron density. The values of the refractive index were determined by the deflection of the laser beam passing through the discharge region. Analysis of the results obtained has shown that the maximum electron density in the dielectric barrier discharge plasma is 10^{19}–10^{20} m^3 [11], which agrees with the results obtained earlier by the method of photometric measurements of shadow patterns for two wavelengths of the probe radiation [12].

In computational modeling of the process of ionized gas flow past a surface, an important role is played by the information on the distribution of electrons in the modeled flow. The aim of the present work is to measure by the optical method the distribution of averaged temperature and density values of electrons in the near-surface high-frequency barrier discharge in the presence of external air flow.

Experimental Equipment and Measuring Techniques. For the investigated object, we used a smooth caprolone plate of thickness 10 mm and surface dimensions 180 × 120 mm. On the pointed front edge on either side of the plate a system of needle electrodes was installed. The electrodes were spaced 3 mm apart and mounted parallel to the surface at a height of 3 mm. The second electrode represented a portion of copper wire covered with fluoroplastic insulation and mounted into the plate parallel to the front edge at a distance of 40 mm from the ends of the needle electrodes.

A high-frequency barrier discharge was formed as a result of applying to the electrodes a high a.c. voltage. The discharge feed circuit diagram is analogous to that presented in [12]. The amplitude value of voltage on the discharge electrodes was varied over the 70–140 kV range.

As a result of the interaction of charged particles with the field of electrodynamic mass forces, in the discharge there appeared a directed gas flow (whose velocity was ~5–10 m/sec) with the formation of a turbulent boundary layer on the plate surface. The process of high-frequency barrier discharge burning was accompanied by a flow over the plate of an air jet flowing out of a nozzle with an outlet section of 15 × 200 mm. The scheme of the experimental setup and the principle of operation of the nozzle were considered in detail in [13]. From a high-pressure line, compressed air was supplied through a system of purifying filters to a receiver of volume 0.2 m^3. Depending on the required flow velocity past the surface, the necessary working pressure was set in the receiver. The nozzle was fed through a line into which the receiver was discharged through a controlled high-speed high-pressure valve. The inves-

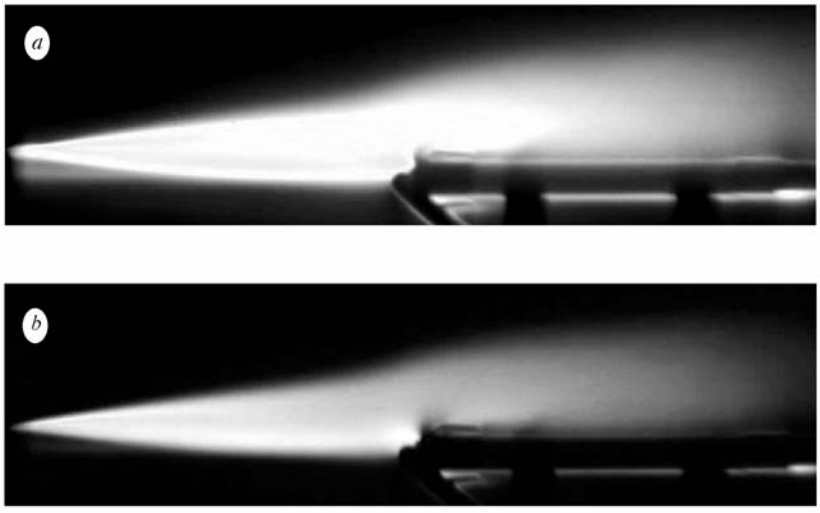

Fig. 2. Shadow patterns of the boundary layer on the plate for two wavelengths: a) λ_r = 650 nm; b) λ_b = 420 nm.

tigated plate was set along the symmetry plane of the jet at a distance of 120 mm from the nozzle exit section. The incident flow velocity was checked by means of a Pitot–Prandtl tube. The jet velocity in the vicinity of the front edge was about 60 m/sec.

The average electron density distribution was investigated by the shadow knife and slit method [14]. The optical scheme of the experimental setup is given in Fig. 1.

Experiments on the investigation of the flow past the plate in the presence of a high-frequency barrier discharge were performed on an IZK-463 mirror-meniscus interferometer adjusted in the regime of a shadow instrument. The focal length of the lens 1 of the receiving part was F = 3213.5 mm at a diameter of the observed field of 800 mm. The width of the slit 2 in the illumination part of the instrument Δx = 0.1 mm. The slit was set parallel to the surface of the plate 3. To average turbulent pulsations in the flow, photography of the shadow patterns was carried out with exposure Δt = 2 sec. In the illumination part of the instrument, two optical filters 4 having the maximum transmission of light at wavelengths λ_r = 650 nm and λ_b = 420 nm were set alternately. Figure 2 shows the shadow patterns of the interaction between a two-dimensional air jet and a barrier discharge obtained for these wavelengths. As follows from visual observations on the shadow device, the presence of the barrier discharge causes a reduction of the incident flow to the plate surface.

Methods and Results of Measurements and Calculations. In the case of sufficiently small angles of deflection of light when transmitted through the investigated inhomogeneities (for example, when light propagates in a turbulent gas flow), it may be assumed approximately that the light beam propagates in straight lines. In the system of rectangular coordinates arranged so that the z axis is directed along the probe radiation propagation and the x axis is perpendicular to the investigated plate, the Euler equations can be written in a simplified form [14]:

$$\tan \varepsilon_x \approx \int_{z_1}^{z_2} \frac{d\{\ln [n(x, y, z)]\}\, dz}{dx}, \quad \tan \varepsilon_y \approx \int_{z_1}^{z_2} \frac{d\{\ln [n(x, y, z)]\}\, dz}{dy}, \tag{1}$$

where the quantities ε_x and ε_y are projections of the angles of deflection of light; z_1 and z_2 are the coordinates of the points of entrance of the light into the optical inhomogeneity and of exit from it.

The slit in the illumination part was set parallel to the plate surface, and the investigated inhomogeneity therewith could be assumed approximately to be two-dimensional; consequently, the function $\frac{\partial n}{\partial x}$ does not depend on the z coordinate and the value of $\frac{\partial n}{\partial y}$ is negligibly small. In so doing, the system of equations (1) reduces to one equation:

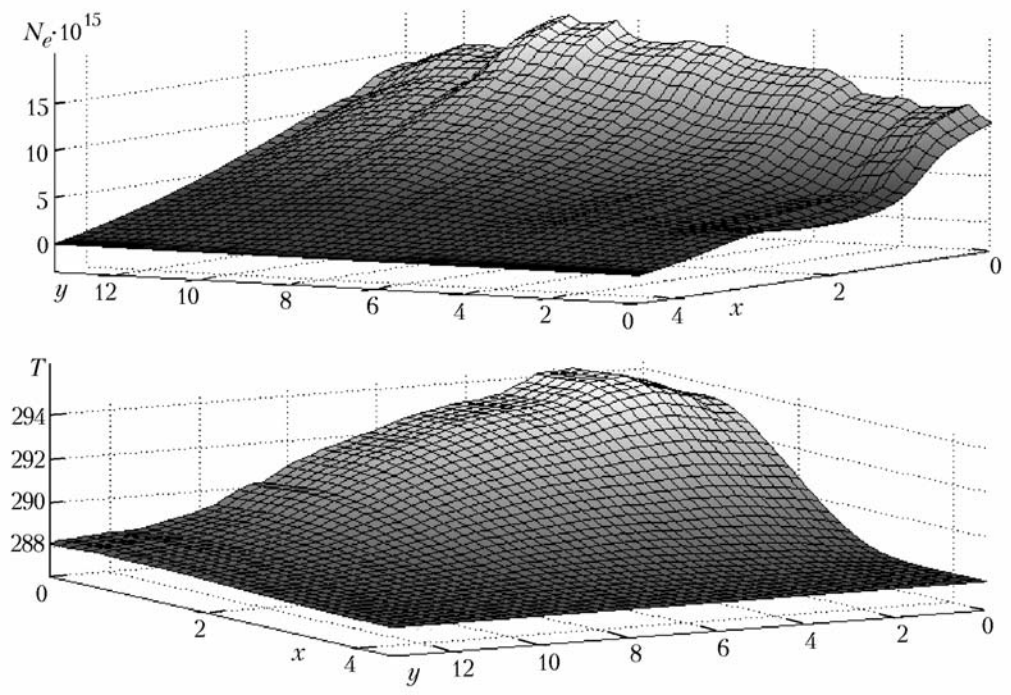

Fig. 3. Three-dimensional distributions of the averaged values of the electron density and temperature in the boundary layer. T, K; N_e, m^{-3}; x, y, mm.

$$\varepsilon_x = \frac{1}{n_0}\frac{\partial n}{\partial x}(z_2 - z_1) - \frac{1}{n_0}\frac{\partial n}{\partial x}\Delta z\,, \tag{2}$$

where Δz is the path length of the light beam in a plane inhomogeneity.

The quantity ε_x is experimentally measurable and is found from the results of photometric measurements of shadow patterns of the air flow past the plate with the use of the formula from [15]

$$\frac{\Delta I}{I_0} = \frac{\varepsilon_x F}{\Delta x}\,, \tag{3}$$

where the intensity I_0 is found from the shadow pattern obtained in the absence of the Foucault knife and ΔI is the intensity difference between the disturbed and undisturbed zones of the shadow pattern of the air flow past the plate in the presence of the Foucault knife.

In determining the intensity values, it is important to note the following fact. The digitized images obtained at wavelengths λ_r and λ_b were recorded in the RGB color representation format using the red, green, and blue color channels for reproducing the image colors. However, such a basic color system is not suitable for direct intensity measurement by formula (3). The HSI color model, whose components are hue, saturation, and intensity, is better suited to the given problem. There exists a one-to-one switch between the RGB and HSI color models, with the sought intensity value in the HSI model being the arithmetic mean of the values of the color channels from the RGB model [16].

The absolute values of the refractive index in the turbulent flow past the plate can be found if its value at some point on the integration line is known. Such a basic value is the refractive index in the undisturbed zone n_0 (i.e., the refractive index in pure air). The results of the integration of Eq. (2) have the form

$$n(x, y) = n(x_0, y) - \int_{x_0}^{x} \frac{\partial n}{\partial x}(x, y)\,dx = n_0 - \frac{n_0}{\Delta z}\int_{x_0}^{x} \varepsilon_x(x, y)\,dx = n_0 - \frac{n_0}{\Delta z}\frac{\xi}{F}\int_{x_0}^{x} \frac{\Delta I(x, y)}{I_0}\,dx\,. \tag{4}$$

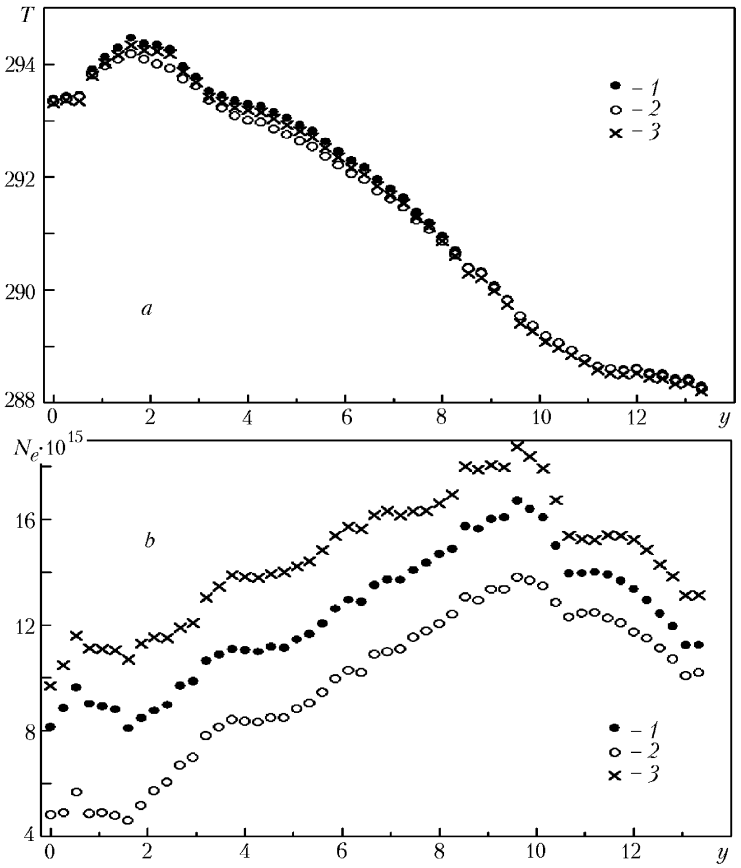

Fig. 4. Distributions of the averaged temperature (a) and densities (b) of electrons along the flow: 1) x = 3 mm; 2) 6; 3) 10. T, K; N_e, m^{-3}; y, mm.

For the digitized image with discrete values of the intensity the integral in formula (4) goes over into a sum where summation is made over all pixels of the image along the x axis.

The refractive index of the plasma depends on both the molecular composition of the gas and the density of free electrons and can be written in the form of the following relation [14]:

$$n - 1 = k\rho\,(1 + \beta T) - K\lambda^2 N_e\,, \tag{5}$$

where

$$K = \frac{e^2}{2\pi m_e c^2} = 4.5 \cdot 10^{-14}\,.$$

Assuming that the flow in the self-similar region of the jet is isobaric, let us rewrite relation (5) in the form

$$n - 1 = (n_0 - 1)\,\frac{T_0}{T} - K\lambda^2 N_e\,. \tag{6}$$

Using the wavelength dependence of the air refractive index [15]

$$n - 1 = \frac{1}{10^6}\left[64.328 + \frac{29498.1}{146 - \dfrac{10^6}{\lambda^2}} + \frac{255.4}{41 - \dfrac{10^6}{\lambda^2}}\right], \tag{7}$$

we can write Eq. (5) for two wavelengths λ_r = 650 nm and λ_b = 420 nm. We obtain a system of two equations for two unknown quantities — the temperature and density of electrons:

$$n_b - 1 = (n_{b0} - 1)\frac{T_0}{T} - K\lambda_b^2 N_e\,, \quad n_r - 1 = (n_{r0} - 1)\frac{T_0}{T} - K\lambda_r^2 N_e\,. \tag{8}$$

Solving the system of equations (8) for the unknown quantities for each pixel of the image, we find the electron temperature and density distributions over the entire flow field. Figure 3 shows the results of calculating the three-dimensional distributions of the averaged values of the temperature and density of electrons over the entire flow field under the plate. The distributions of the averaged values of the temperature and density of electrons along the flow for three different distances from the plate surface are shown in Fig. 4.

Conclusions. The obtained values of the electron density are comparable in magnitude to the corresponding values for the glow discharge. Since the presence of external air flow past the plate prevents discharge contraction and the formation of streamers, the data presented are somewhat higher compared to the analogous results obtained in the absence of the air flow [12]. In this case, a monotonic downstream increase in the electron density within the discharge gap and its subsequent decrease due to the processes of electron-ion recombination and turbulent mixing are observed. From the temperature distribution plot it is seen that heating of the gas occurs in a small region just behind the needle electrodes. Then there is a monotonic decrease in the temperature as a result of the turbulent mixing with the ambient air.

Thus, unlike the barrier discharge with a self-induced flow where a wavy change in the electron density and temperature occurs, the presence of external air flow leads to a maximum in the average temperature distribution in the vicinity of the needle electrodes, and a maximum of the average electron density in the region of the opposite electrode.

This work was supported by the Belarusian Republic Basic Research Foundation and the Russian Basic Research Foundation, project No. T08R-222.

NOTATION

e, electron charge, C; F, focal length of the lens, mm; I, radiation intensity, W/m^2; k, Gladstone–Dale constant, m^3/kg; m_e, electron mass, kg; n, refractive index of the medium; t, time, sec; T, averaged temperature of the electron, K; N_e, electron density, m^{-3}; V, voltage on discharge electrodes, kV; x, y, z, system of Cartesian coordinates, m; β, thermal coefficient of volumetric expansion, K^{-1}; ε, deflection angle of light, seconds of arc; λ, probe radiation wavelength, nm; ρ, medium density, m^{-3}. Subscripts: 0, undisturbed medium; b, blue light; r, red light.

REFERENCES

1. J. R. Roth and Xin Dai, Optimization of the aerodynamic plasma actuator as an electrohydrodynamic (EHD) electrical device, *44th AIAA Aerospace Sciences Meeting and Exhibit*, 9–12 January 2006, Reno, Nevada, AIAA 2006-1203.
2. D. V. Roupassov, I. N. Zavyalov, and A. Yu. Starikovskii, Boundary layer separation plasma control using low-temperature non-equilibrium plasma of gas discharge, *44th AIAA Aerospace Sciences Meeting and Exhibit*, 9–12 January 2006, Reno, Nevada, AIAA 2006-373.
3. P. Khramtsov, O. Penyazkov, M. Chernik, I. Shatan, and I. Shikh, Effect of surface high-frequency barrier discharge on a flat plate drag reduction, *3rd Int. Workshop "Nonequilibrium Processes in Combustion and Plasma-Based Technologies,"* Minsk (2008), pp. 44–47.
4. G. I. Font, S. Jung, C. L. Enloe, and T. E. McLaughlin, Simulation of the effects of force and heat produced by a plasma actuator on neutral flow evolution, *44th AIAA Aerospace Sciences Meeting and Exhibit*, 9–12 January 2006, Reno, Nevada, AIAA 2006-0167.
5. O. G. Penyazkov, P. P. Khramtsov, M. Yu. Chernik, I. N. Shatan, and I. A. Shikh, Influence of the plasma of a high-frequency barrier discharge on the structure of the dynamic boundary layer on a flat surface, *Inzh.-Fiz. Zh.*, **81**, No. 1, 55–61 (2008).

6. G. I. Font, C. L. Enloe, T. E. McLaughlin, and D. Orlov, Plasma discharge characteristics and experimentally determined boundary conditions for a plasma actuator, *44th AIAA Aerospace Sciences Meeting and Exhibit*, 9–12 January 2006, Reno, Nevada, AIAA 2006-188.
7. O. G. Penyazkov, P. P. Khramtsov, M. Yu. Chernik, I. N. Shatan, and I. A. Shikh, Influence of ionic wind on the structure of a dynamic boundary layer on a flat plate, in: *Proc. 6th Minsk Int. Forum "Heat and Mass Transfer–MIF-2008"* [in Russian], Minsk (2008), ISBN 978-985-6456-60-5, paper No. 1.48.
8. A. A. Sidorenko, B. Yu. Zanin, B. V. Postnikov, A. D. Budovsky, A. Yu. Starikovskii, D. V. Roupassov, I. N. Zavialov, N. D. Malmuth, P. Smereczniak, and J. S. Silkey, Pulsed discharge actuators for rectangular wing separation control, *44th AIAA Aerospace Sciences Meeting and Exhibit*, 9–12 January 2006, Reno, Nevada, AIAA 2007-941.
9. D. M. Orlov, T. C. Corke, and M. P. Patelz, Electric circuit model for aerodynamic plasma actuator, *44th AIAA Aerospace Sciences Meeting and Exhibit*, 9–12 January 2006, Reno, Nevada, AIAA 1206-2006.
10. C. L. Enloe, T. E. McLaughlin, G. I. Font, and J. W. Baughn, Frequency effects on the efficiency of the aerodynamic plasma actuator, *44th AIAA Aerospace Sciences Meeting and Exhibit*, 9–12 January 2006, Reno, Nevada, AIAA 2006-166.
11. A. V. Likhanskii, M. N. Shneider, S. O. Macheret, and R. B. Miles, Modeling of interaction between weakly ionized near-surface plasmas and gas flow, *44th AIAA Aerospace Sciences Meeting and Exhibit*, 9–12 January 2006, Reno, Nevada, AIAA 2006-1204.
12. P. P. Khramtsov, O. G. Penyazkov, M. V. Doroshko, M. Yu. Chernik, and I. A. Shikh, Shadow method for measuring the average electron density in an ionized gas flow induced by a high-frequency barrier discharge, *Inzh.-Fiz. Zh.*, **82**, No. 2, 364–370 (2009).
13. P. P. Khramtsov, O. G. Penyazkov, V. M. Grishchenko, M. Yu. Chernik, I. N. Shatan, and I. A. Shikh, Aerodynamic drag of a plate in an ionized gas flow induced by a near-surface high-frequency barrier discharge, *Inzh.-Fiz. Zh.*, **82**, No. 4, 726–731 (2009).
14. L. A. Vasil'ev, *Shadow Methods* [in Russian], Nauka, Moscow (1968).
15. R. Huddlestone and S. Leonard (Eds.), *Plasma Diagnostics* [Russian translation], Mir, Moscow (1967).
16. R. C. Gonzales, R. E. Woods, and S. L. Edding, *Digital Image Processing Using MATLAB* [Russian translation], Tekhnosfera, Moscow (2006), pp. 206–253.